Design optimization of moiré interferometers for rapid 3-D manufacturing inspection

Steven Dubowsky
Krisztina Holly
Annie L. Murray
Joseph M. Wander

Mechanical Engineering Department
Massachusetts Institute of Technology
Cambridge, MA

ABSTRACT

While moiré interferometry has been recognized as a promising technique for 3-D automated inspection, it has not been widely used because designing a moiré interferometer for a given inspection task can be difficult. Here mathematical models of the projection moiré process are developed which permit the design of inspection systems. The resulting equations have been combined with numerical optimization techniques to yield software which optimizes a system for a given task. An application of the technique with experimental verification is presented.

1. INTRODUCTION

Automated and flexible inspection is an essential element in modern manufacturing. For this field to achieve its full potential one area which requires technical development is the inspection of three-dimensional (3-D) surfaces. For some time, moiré interferometry has been recognized as a promising technique for 3-D inspection[1]. However, the technique has not been widely put into practice because designing and tuning a moiré interferometer to meet the requirements of a given inspection task can be difficult. This difficulty is due in large measure to the lack of design paradigms for such systems. This paper presents an analytical method to enable moiré interferometers to be designed and optimized for a given inspection task is presented.

Other methods are available to inspect the three-dimensional geometry of parts. However, in many applications they do not offer the advantages that can be achieved with moiré interferometry. Contact probe measurement is tedious, often inaccurate, and can lead to sensor wear and part damage; laser triangulation and structured light methods are computer time-intensive; and conventional computer vision techniques are limited by pixel resolution and only analyze the 2-D outlines of the parts[2]. Moiré interferometry is not subject to these limitations. Using the principle of interference, a moiré interferometer can act as an error amplifier so that small errors will easily be detected even by low-resolution vision systems, avoiding the pixel limitation problem. Moiré interferometry fundamentally requires less computer time than methods such as laser triangulation, so it has greater potential for rapid on-line inspection. In addition, since the parameters of a moiré interferometer can easily be changed, it lends itself to rapid prototyping inspection. Despite all of these advantages, moiré interferometry has not yet been exploited to its full potential. Moiré systems are difficult to design and adjust. Applying this technology can be a time consuming and even frustrating trial and error process, negating its inherent flexibility and advantages.

In this paper an analytical basis appropriate for designing and optimizing moiré inspection systems is presented. The projection moiré interferometry process is modeled mathematically to yield a set of equations describing the moiré fringes that would be produced by a given interferometer system when it examines a given

object with specified tolerances. These equations also permit the design of an inspection system, to achieve the desired measurement sensitivity. The method has been implemented in a software package with numerical optimization techniques to optimize a moiré interferometer design for a given application. The paper also presents an application of this technique with experimental verification.

2. THE TECHNIQUE AND ITS ANALYTICAL BASIS.

Moiré patterns are formed when two similar high frequency patterns of light and dark are superimposed[3]. Slight differences between the two patterns are magnified into easily detectable low spatial frequency fringes that compose the moiré pattern. In projection moiré interferometry (see Figure 1), a grid pattern is projected onto an object. The grid pattern on the object surface, modified by the object's shape, is then observed by the viewing system through another grid. Such moiré processes can be modeled analytically[4,5] and simulated[6]. The model is a function of the reflectivity of the object's surface -- diffuse or specular -- and the nature of the optics of the system. Here it is assumed that the objects have surfaces with diffuse characteristics and that the optics are focal rather than collimated. Models for specular surfaces and collimated optics have also been developed[5].

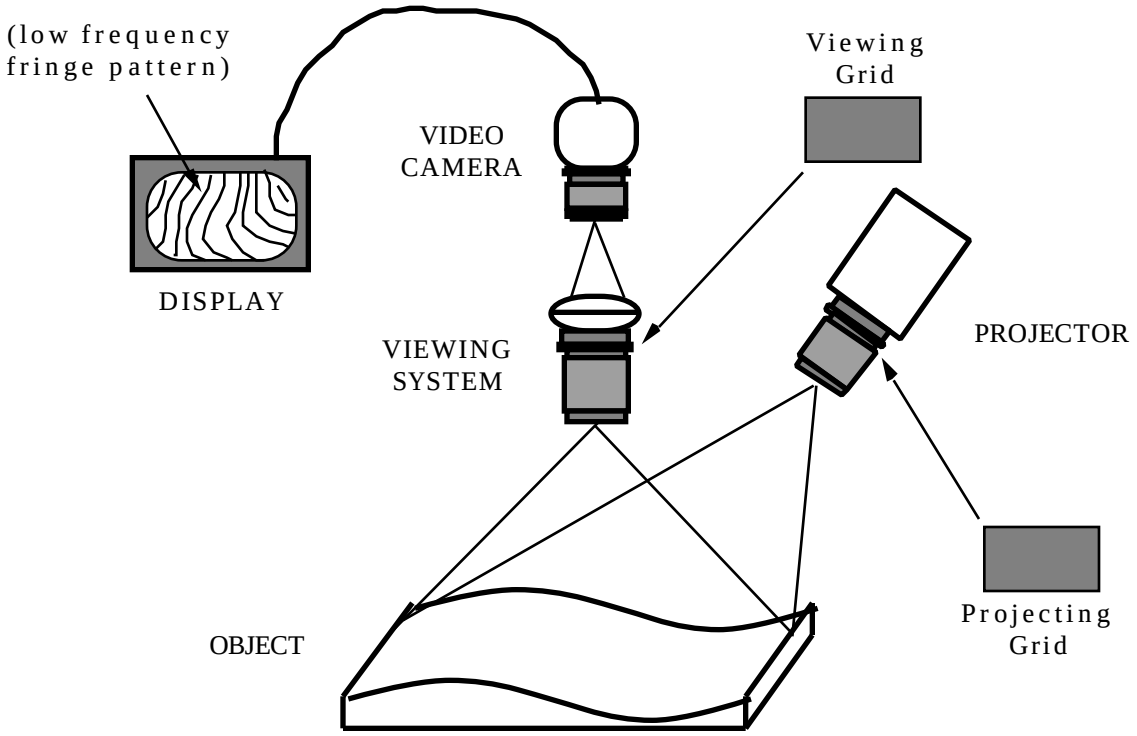

Figure 1. A Projection Moiré Interferometer

Projection moiré interferometry can be represented using the concept of "equiorder surfaces"[7]. If the planes of light produced by the grid pattern of the projection system are permitted to intersect with analogous planes "projected" by the viewing grid pattern, a family of surfaces in space can be constructed, such as shown in Figure 2. These smooth, imaginary surfaces have been called "equiorder surfaces" and are an effective a tool for understanding the moiré process. Each surface is associated with a nondimensional number called a Fringe Order (*FO*) number. It can be shown that where an object intersects an equiorder surface in space, a fringe will appear

on the image plane of the viewing system at that point. Hence, finding the intersection between the object and the imaginary equiorder surfaces will predict the resulting moiré pattern as seen by the viewing system[7].

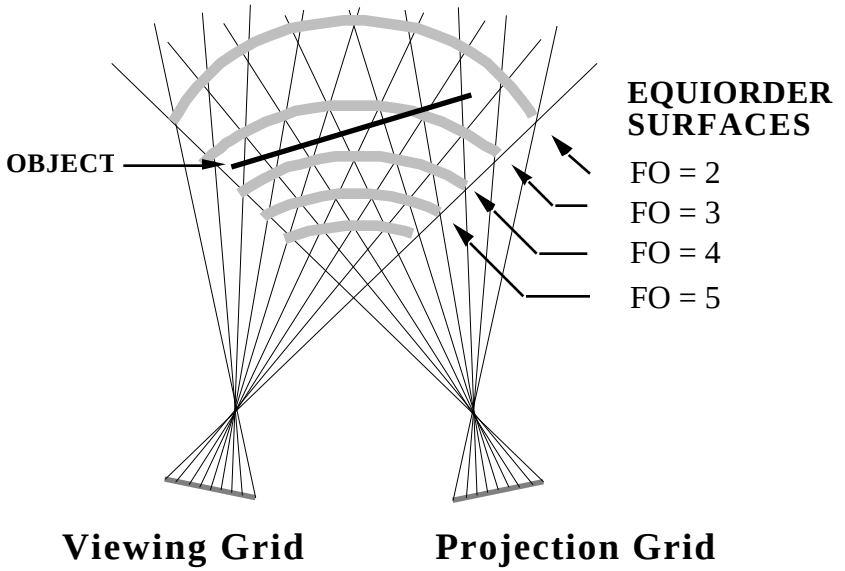

Figure 2. Equiorder Surfaces

It also can be shown that the equations of the equiorder surfaces can be written in terms of the parameters of the system as follows[5,8,9]:

$$w(x, y, z, FO) = Ax^2 + By^2 + Cz^2 + Dxy + Eyz + Fxz + Gx + Hy + Iz = 0 \quad (1)$$

where:

$$A = S_v P_p \sin\zeta \cos\alpha_v$$

$$B = 0.0$$

$$C = P_v P_p (FO + \varphi_v - \varphi_p) \cos\zeta + S_p P_v \sin\zeta \cos\alpha_p$$

$$D = S_v P_p \sin\zeta \sin\alpha_v$$

$$E = S_v P_p \cos\zeta \sin\alpha_v - S_p P_v \sin\alpha_p$$

$$F = P_v P_p (FO + \varphi_v - \varphi_p) \sin\zeta + S_v P_p \cos\zeta \cos\alpha_v - S_p P_v \cos\zeta \cos\alpha_p$$

$$G = - S_v P_p (x_{po} \sin\zeta + z_{po} \cos\zeta) \cos\alpha_v$$

$$H = - S_v P_p (x_{po} \sin\zeta + z_{po} \cos\zeta) \sin a_v$$

$$I = - P_v P_p (x_{po} \sin\zeta + z_{po} \cos\zeta (FO + \varphi_v - \varphi_p) + S_p P_v (x_{po} \cos\zeta - z_{po} \sin\zeta) \cos\alpha_p$$

The coordinates x_{po}, y_{po}, and z_{po} in the above equation define the location of the projection system optic center in system coordinates, which are located at the viewing system optic center as shown in Figure 3. The angle ζ and the focal distances S_V and S_p are also defined in Figure 3. The variables α_p, α_v, φ_p, φ_v, P_p, and P_v are the angle, phase, and constant pitch of the straight-line projection and viewing grids, respectively, as defined with respect to their local coordinate frames, see Figure 4.

Using equation (1) and a mathematical representation of the object, such as a CAD model, equations can be written to predict the fringe patterns given the properties of the moiré interferometer[8]. By comparing the

actual inspected fringe pattern to the calculated one, a better understanding of the geometry of the real part and how it differs from the ideal CAD model can be obtained. In order to analyze actual object geometry using this inspection technique, it is necessary to be able to determine object coordinates from the moiré pattern formed on the image plane. The above equations can be rewritten to express the object coordinates in terms of the fringe order and location on the image plane[5].

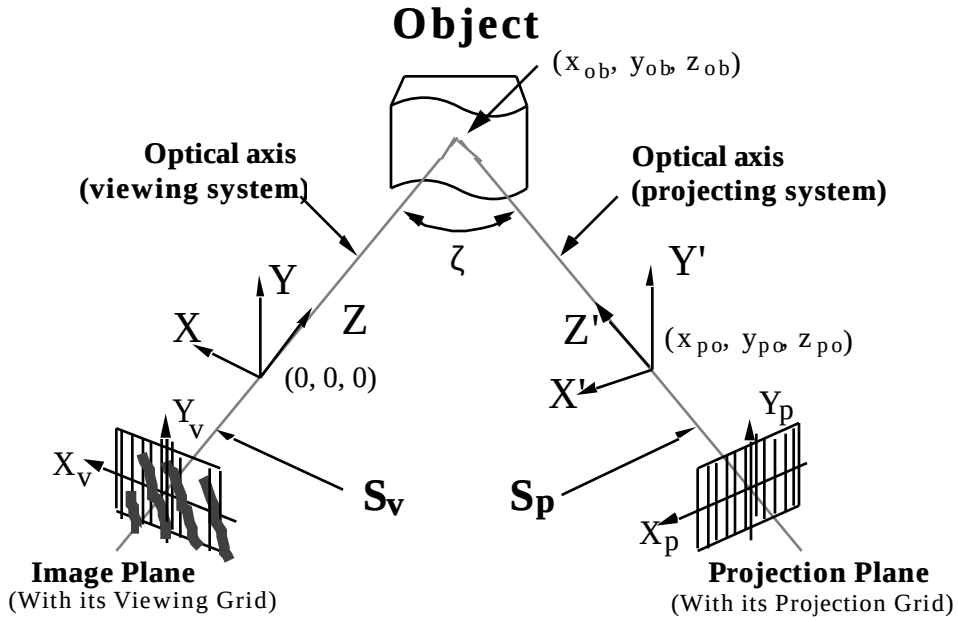

Figure 3. Projection Moiré Interferometer System Coordinates

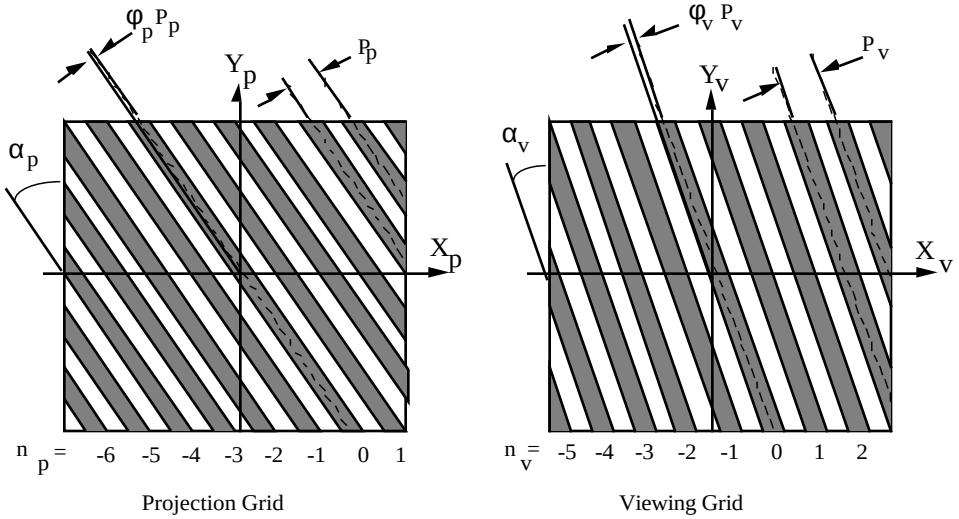

Figure 4. Projection and Viewing Grids Parameters

This analytical model of the moiré process has been validated using a ray-tracing simulation and laboratory experiments[5,6]. Figure 5 shows analytically predicted fringes for two different orientations of a flat plate in a given moiré interferometer. Also shown are the simulated and experimental results for the same cases. The agreement obtained gives confidence in the analytical model. For a more detailed account of this verification see references 5 and 6.

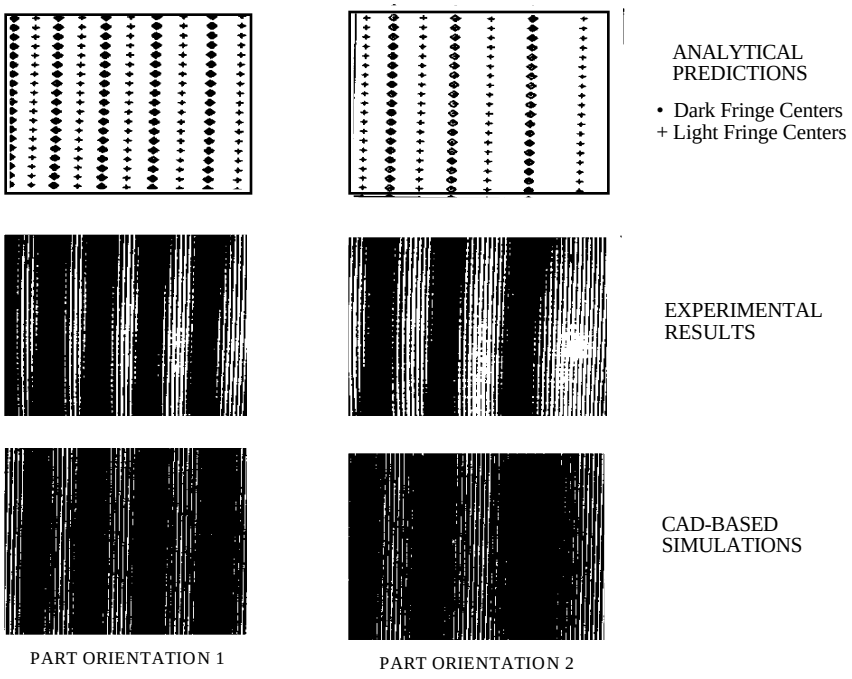

Figure 5. Simulation and Experimental Verification of the Analytical Model

3. DESIGN OPTIMIZATION OF MOIRÉ INTERFEROMETERS

As discussed above, a major difficulty in using moiré interferometers for the inspection of parts in manufacturing is that they can be difficult to design. For the interferometer to be effective, its parameters must be chosen so that measurable fringes are obtained and that the range of expected errors in the part's geometry can be readily estimated from the observed fringes. In addition it is highly desirable that the size of the interferometer be appropriate for the task and that it can be constructed with readily available components. In this study analytical methods for designing moiré systems were investigated to eliminate the need for costly and inadequate trial and error methods. Using the concept of equiorder surfaces, the analytical models of the moiré process discussed above, and numerical optimization methods an automated method for the optimal design of moiré interferometers has been developed. The parameters of the interferometer are optimized to adjust the sensitivity and scale of the inspection system to the tolerance and scale of a specified inspection task.

The concept is to design the interferometer so that the equiorder surfaces roughly surround the object being inspected, where the distance between the part and the surfaces is approximately the size of the dimensional tolerance on the part. In this way, out-of-tolerance conditions would cause fringes so unacceptable errors could be quickly identified. It might be noted that we have developed an optimization method, to follow the interferometer optimization, that creates curved grids rather than simple straight line grids, which more closely contours the shape of the equiorder surfaces to the shape of the object[9]. A discussion of this extension is beyond the scope of this paper.

There are fifteen interferometer parameters which can be optimized. They are (referring to Figure 3): the object position (x_{ob}, y_{ob}, z_{ob}) and the projection system location (x_{po}, y_{po}, z_{po}); the angle ζ; the focal distances S_v and S_p; and the six parameters which describe the grid configurations (α_p, α_v, φ_p, φ_v, P_p, and P_v shown in Figure 4). Following standard numerical optimization methods a cost function is developed. This cost function is

stated in terms of the object and equiorder surface characteristics. First, to have the EO surfaces follow the part surface as closely as possible, costs are assigned to the angle between the EO surface normal and the part surface normal, and to the difference between curvatures of the EO surfaces and the part. In some cases, we may want to set the equiorder surfaces at an angle to the part instead, and this will be discussed in Section 4. The spacing between the EO surfaces is driven by the cost function to be some function of the tolerance to be measured. The cost function also includes a term to insure that the combined fields of view of the projection and viewing systems, R_I, is the same size or larger than the object surface size represented by its "characteristic length," R_{ob}.

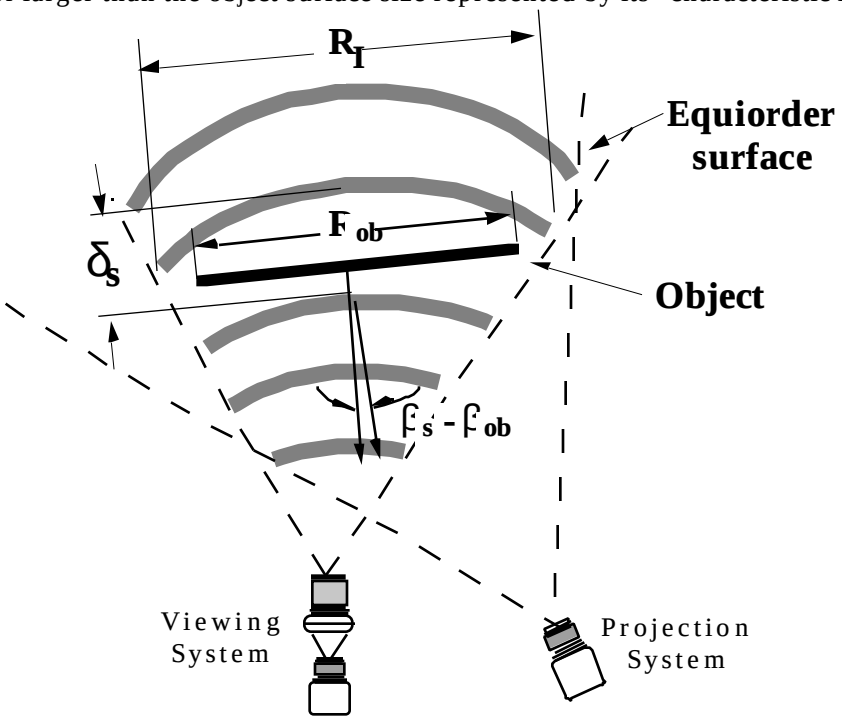

Figure 6: Variables Used in Cost Function

The cost function contains terms to insure that the interferometer will have good optical characteristics. To avoid optical distortion, it has been suggested that[4]:

$$P_v \, S_p = P_p \, S_v \, . \tag{2}$$

The cost function may also contain other optical constraints. For example, the difference between grid line angles, φ_p and φ_v, must be less than 45° to ensure the formation of clear fringes, the viewing and projecting systems must be located such that they don't obscure each other, and the part must be at least one focal length from the optic centers. In addition, the grid pitches may have bounds or the grid size may be specified to one of several standard sizes. The resulting cost function will have the form:

$$F = a_1(R_I - R_{ob})^2 + a_2(\delta_s - 2tol)^2 + a_3(\beta_s - \beta_{ob})^2 + a_4(\kappa_s - \kappa_{ob})^2 + a_5\left(\frac{P_v \, S_p}{P_p \, S_v} - 1\right)^2 + \text{Optical Constraints} \tag{3}$$

where a_1-a_5 are weighting factors; R_I and R_{ob} are the widths of the interference region and the part, respectively; δ_s is the distance between the equiorder surfaces; tol is the tolerance of the inspection; $\beta_s - \beta_{ob}$ is the angle between the equiorder surface and object normals; and κ_s and κ_{ob} are the curvatures of the EO surface and the object surface (see Figure 6).

The variables used in the cost function (3) can be derived from the object characteristics and from the equiorder surface equation, which is dependent on the variables that are optimized. For example, β_S is found by calculating the direction of the normal to an equiorder surface at an evaluation point, (x_1, y_1, z_1), close to the center of the object. This is given by the gradient of the equiorder surface divided by its magnitude:

$$\hat{n}_S = \frac{w}{|w|} \tag{4}$$

where the magnitude

$$|w| = \sqrt{\left(\frac{\partial w}{\partial x}\right)^2 + \left(\frac{\partial w}{\partial y}\right)^2 + \left(\frac{\partial w}{\partial z}\right)^2}\,. \tag{5}$$

The partial derivatives in equation (5) can be written in the following form:

$$\frac{\partial w}{\partial x} = C_1 x_1 + C_2 y_1 + C_3 z_1 + C_4 \tag{6}$$

where C_1-C_4 are coefficients written in term of the optimization parameters. For example,

$$C_1 = -2\frac{P_p S_v}{S_p P_v} \sin\zeta \cos\alpha_v\,. \tag{7}$$

The other coefficients in equation (6) can also be written in terms of the interferometer parameters being optimized. The spacing between the surfaces, δ_S, the surface curvature, κ_S, and the size of the interference region, R_I, can also be calculated in the same manner as β_S[8]. The object characteristics defined by the cost function, such as the curvature, can be calculated from the known nominal geometry of the part. The computer implementation of the optimization process is illustrated in Figure 7. It uses an optimization subroutine in the IMSL library called "ZXMWD()" to minimize the cost function[10]. The subroutine FUNCT() specifies to ZXMWD() the cost function to be minimized.

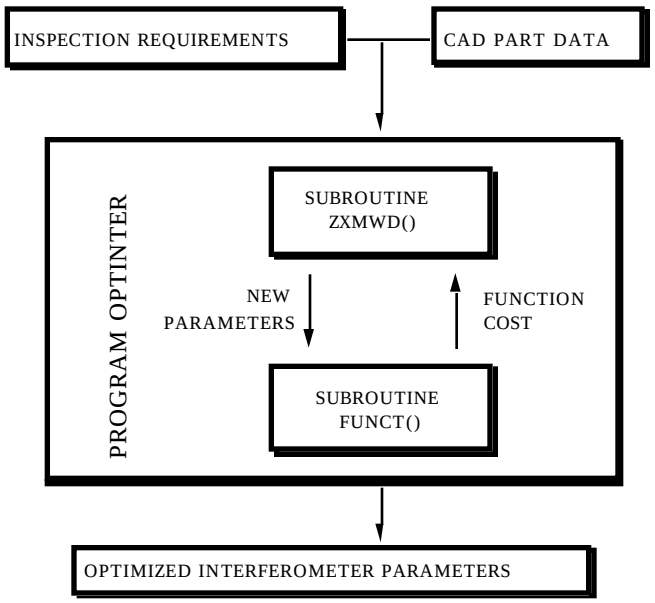

Figure 7: Computational Flowchart

The following example shows the results of an optimization of EO surfaces optimized for an object with a multi-faceted surface (see Figure 8). Here, by segmenting the viewing and projection grids it has been possible to place sections of the EO surfaces parallel to sections of the object surface one half the tolerance away. As mentioned before, we have also extended this work to inspecting continuous curved surfaces using spline grids[9].

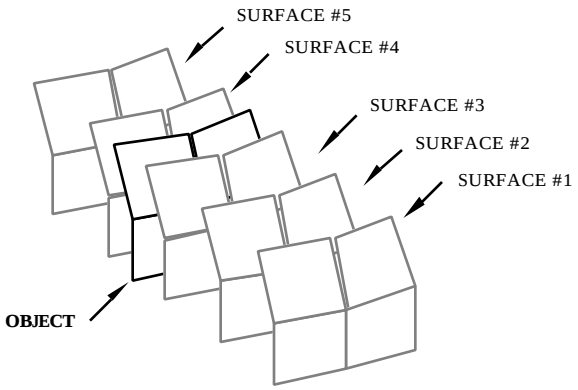

Figure 8: Equiorder Surfaces After Optimization

4. AN APPLICATION

In this application, an embossment on diesel engine head gaskets were inspected (see Figure 9). The task was to measure the height of the gasket embossment within the manufacturing tolerance of 25%. The embossment was a tenth of an inch wide and its height varied from part to part between 0.006 and 0.012 inches.

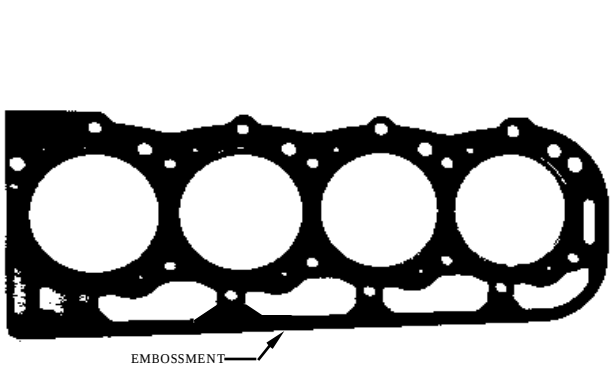

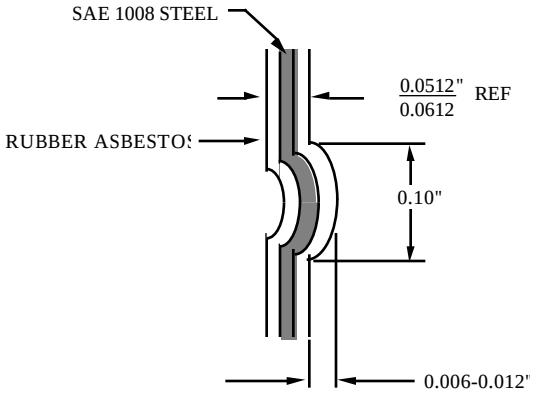

a. Gasket b. Gasket Embossment Cross-Section

Figure 9: A Diesel Engine Head Gasket Inspection Task

As discussed earlier, one moiré inspection approach places the EO surfaces parallel to the object surface (see Figure 8). This is most suited for measuring whether a part is within tolerance. The gasket inspection task, however, requires the height measurement of different embossments. In this case, by flattening the EO surfaces (making their curvature zero) and placing them at a specified angle from the part ($\beta_s - \beta_{ob}$), evenly spaced lines will appear on the surface of the part (see Figure 10). Any changes in the part height will shift the fringes in proportion to the height change.

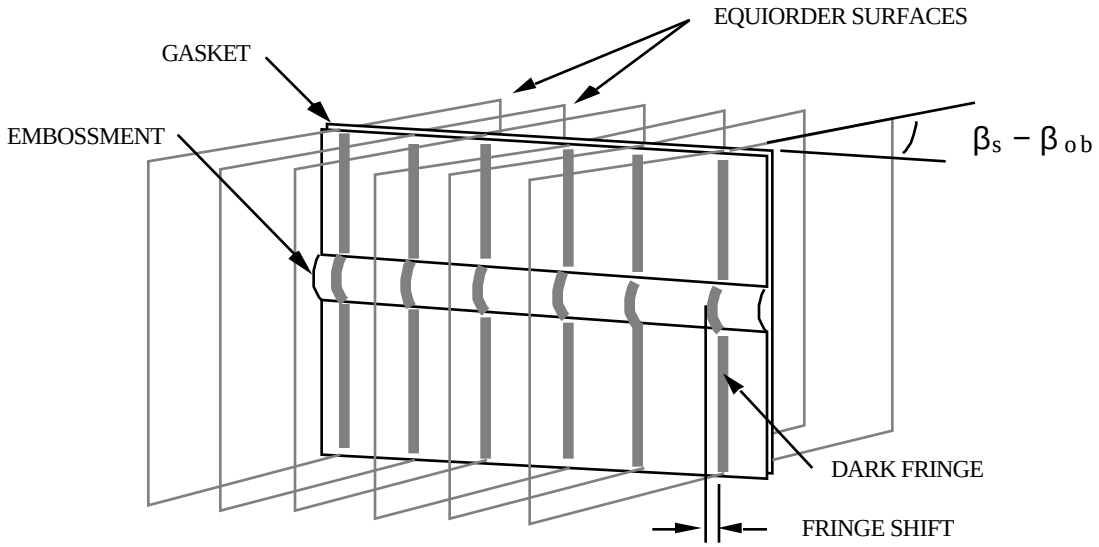

Figure 10: Placing the Equiorder Surfaces

For this task, it was desired that an embossment 0.012 inches high would shift a section of the moiré pattern by one fringe. The sensitivity of the interferometer is defined as[11]:

$$\text{sensitivity} = \frac{\Delta P_{\text{fringe}}}{H} = \frac{\text{fringe shift}}{\text{gasket height}}$$

Therefore, the interferometer was designed with a sensitivity of 83 fringes/inch. The gasket was defined so that its surface normal would be parallel to the viewing system axis, and the EO surface normals were selected to be at an angle of 16.5° from the gasket surface normal in the x-z plane (see Figure 10). Such a selection can be accommodated by a minor change in the cost function, equation (3). These above choices lead to a desired equiorder surface spacing of 0.294 mm. The resulting interferometer parameters are given in Table 1.

Table 1. Interferometer Parameters

Xc	Zc	Xo	Zo	ζ	Sp	Sv	Pp	Pv
0.0 mm	141.0 mm	-90.0 mm	1.8 mm	33°	70.0 mm	78.8 mm	0.169 mm/line	0.254 mm/line

Each gasket was placed into the moiré interferometer and inspected by measuring the fringe shift between the gasket and embossment surfaces (see Figure 10). The latter part of this process was implemented on an Automatix Autovision II vision system. These measurements were then compared to direct mechanical measurements of the heights. The results are shown in Figure 11. The accuracy of this technique was measured between 0-23%, which is within the specifications. The apparatus used in this experiment were quite simple, and greater accuracy could have been obtained without excessive cost.

It might be noted that accurate fixturing was not necessary in this task because in each case the height of the gasket's embossment was measured with respect to the gasket itself. It is a common characteristic of many inspection tasks that a feature needs to be measured relative to another feature on the same part.

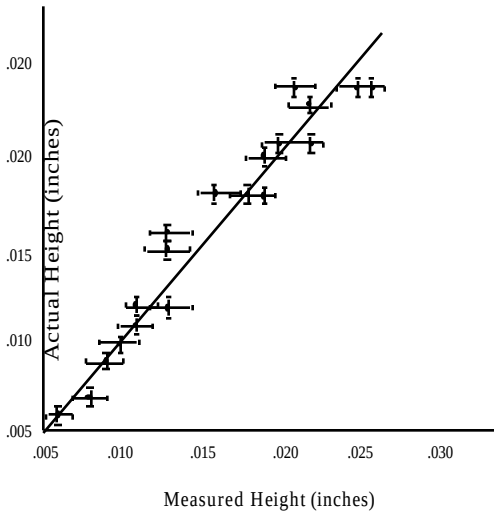

Figure 11: Plot of Optically Measured Embossment Heights vs. Actual Heights.

5. CONCLUSIONS

The practical use of moiré inspection techniques is limited due to the difficulty in designing these systems for a given task. A mathematical model of the projection moiré process has been combined with numerical optimization techniques in a computer-aided design software package for moiré interferometers. We believe this work demonstrates that effective automated methods can be developed to aid in designing moiré inspections systems for specific tasks. Such CAD tools would enable industry to use moiré inspection systems more successfully. The effectiveness of the approach is demonstrated experimentally using the task of inspecting an engine gasket.

6. ACKNOWLEDGEMENTS

The support of this research by the *MIT Leaders for Manufacturing Program* and the *Martin Foundation* (through K. Holly's Fellowship) are acknowledged. The authors also wish to recognize the important contributions of M. Sullivan, R. Leonard, and E. Reidemeister to this work .

7. REFERENCES

1. Brooks, R. E., and Heflinger, L. O.,"Moiré Gauging Using Optical Interference Patterns," *Applied Optics*, Vol. 8, No. 5, May 1969, pp 935-939.

2. Martin, J. M., "Seeing a Payoff Now," *Manufacturing Engineering*, October 1988, pp 47-49.

3. *The Motograph Moving Picture Book*, Bliss, Sands & Co., London, 1898.

4. Chiang, C., "Moiré Topography," *Applied Optics*, Vol. 14, No. 1, January 1975, pp. 177-179.

5. Wander, J.M., *The Application of Moiré Interferometry to Automated 3-Dimensional Inspection*, MS Thesis, Department of Mechanical Engineering, MIT, 1985.

6. Leonard, R., *Application of Moiré Techniques to Manufacturing Inspection*, Master of Science Thesis, Department of Mechanical Engineering, MIT, December 1984.

7. Idesawa, M., Toyohiko Y., and Takashi S., "Scanning Moiré Method and Automatic Measurement of 3-D Shapes," *Applied Optics*, vol. 16, 1977, no. 8, pg 2152.

8. Murray, A.L., *Development of Computer-Based Methods for the Design of Automated Inspection Systems Using Moiré Interferometry*, MS Thesis, Department of Mechanical Engineering, MIT, 1986.

9. Reidemeister, E.P., *Automated Visual Inspection of General Curvature Surfaces Using Moiré Interferometry*, MS Thesis, Department of Mechanical Engineering, MIT, August 1988.

10. *IMSL Library Reference Manual*, 9th Edition, International Math and Science Libraries, Houston, TX, 1982, pp. ZXMWD-1-3.

11. Sullivan, M., *A Demonstration of the Feasibility of a Moiré Fringe Based Method for Inspection*, BS Thesis, Department of Mechanical Engineering, MIT, June 1985.